Terahertz-Band MIMO Systems: Adaptive Transmission and Blind Parameter Estimation

Mohamed Habib Loukil, *Student Member, IEEE,* Hadi Sarieddeen, *Member, IEEE,*
Mohamed-Slim Alouini, *Fellow, IEEE* and Tareq Y. Al-Naffouri, *Senior Member, IEEE*

***Abstract*—We consider the problem of efficient blind parameter estimation in terahertz (THz)-band ultra-massive multiple-input multiple-output (UM-MIMO) systems. UM-MIMO antenna arrays are crucial to overcoming the distance problem in THz communications. Following recent advancements in THz transceiver design, such arrays are intrinsically compact and reconfigurable. We propose dynamically tuning the modulation types, operating frequencies, and indices of transmitting antenna elements for efficient resource utilization in THz UM-MIMO systems. Furthermore, we propose THz-specific signal processing techniques at the receiver side for blindly detecting the transmission parameters. In particular, we propose a low-complexity antenna index, frequency index, modulation mode, and modulation type detectors, and we study the complexity and performance tradeoffs of the proposed schemes.**

***Index Terms*—THz communications, ultra-massive MIMO, adaptive transmission, modulation classification, blind estimation.**

I. Introduction

THz communications play an essential role in the upcoming sixth-generation (6G) of wireless mobile communications [2], with envisioned applications at the intersection of communications, sensing, imaging, and localization [3]. Unlike the millimeter-wave (mmWave) band, exploiting the large available bandwidth at the THz band (0.3 – 10 THz) promises to support terabit/second data rate demands. As THz signal generation, modulation, and radiation methods are maturing, the corresponding THz channel and noise models are emerging, which advocates new research directions on THz-specific signal processing techniques [4]. Recent advancements in electronic and photonic technologies are closing the gap in THz transceiver design. In particular, since satisfying emerging system-level properties requires designing efficient, programmable, and reconfigurable devices, integrated hybrid electronic-photonic systems are emerging [5], as well as plasmonic solutions based on new materials such as graphene [6]. In order to make the best use of resources, a large number of transmission parameters can be adapted [7] in a THz UM-MIMO cognitive radio configuration. In particular, modulation modes, operating frequencies, and active antenna indices can be altered in real-time for each antenna element (AE).

This letter is accepted at IEEE Communications Letters. Further details are available in [1]. All authors are with the Division of Computer, Electrical and Mathematical Sciences and Engineering, King Abdullah University of Science and Technology, Thuwal 23955-6900, Saudi Arabia. (e-mail: mohamedhabib.loukil@kaust.edu.sa; hadi.sarieddeen@kaust.edu.sa; slim.alouini@kaust.edu.sa; tareq.alnaffouri@kaust.edu.sa). This work was supported by the KAUST Office of Sponsored Research.

Two modulation modes can be distinguished: carrier-based modulation (CBM) and pulse-based modulation (PBM). With CBM, the transmitter and the receiver tune to a specific frequency of operation. Since the available THz spectrum is divided into many sufficiently large slots because of molecular absorption, multiple single-carrier transmission schemes over these slots are favored over the much more complex orthogonal frequency-division multiplexing (OFDM) [4]. For PBM, trading short femtosecond-long pulses of few milli-watts [8] is effectively a single-carrier modulation with a frequency response that covers the entire THz band. Due to hardware constraints, sending continuous THz waves of high spectral efficiency is harder and more energy-consuming. Nevertheless, adaptive THz systems can hop over CBM and PBM, as well as over different modulation types within CBM, such as M-ary quadrature amplitude modulations (M-QAMs) and M-ary phase shift keyings (M-PSKs). Instead of adding reference signals that periodically update the receiver on parameter changes, a spectrally-efficient and secure solution is to blindly estimate these parameters at the receiver, prior to data detection. In this letter, we extend the work in [7] on THz-band spatial modulation (SM), and propose a fully adaptive THz UM-MIMO system. We propose blind parameter estimators that complement adaptive transmission at the receiver side. In particular, we propose a tertiary hypothesis test based on power comparison for antenna index and modulation mode detection and derive the corresponding closed-form expressions of error probabilities. We further propose low-complexity frequency index detectors and modulation type estimators.

Regarding notation, bold upper case, bold lower case, and lower case letters represent matrices, vectors and scalars, respectively. $\mathbf{I}_N$ and $\mathbf{0}_N$ are the identity matrix and null vector of size N, respectively. $|\cdot|$ denotes scalar norm or set cardinality and $\Pr(\cdot)$ denotes the probability function. $\mathcal{CN}(\boldsymbol{\mu}, \boldsymbol{\Gamma})$ denotes a complex normal distribution of mean μ and covariance matrix $\boldsymbol{\Gamma}$. $\chi^2(N)$ denotes a chi-square distribution with N degrees of freedom and $\chi^2(N, \lambda)$ stands for a non-central chi-square distribution with a non-centrality parameter λ.

II. System Model and Problem Formulation

We consider a system that consists of two arrays of subarrays (AoSAs) of AEs, one at the transmitter and another at the receiver, consisting of $M_t \times N_t$ and $M_r \times N_r$ sub-arrays (SAs), respectively. We assume that each SA is composed of Q×Q AEs, and that two adjacent SAs are separated by a distance Δ, and two adjacent AEs are separated by a

distance δ. The resultant configuration can be described as a "large" (doubly-massive) $M_t N_t \mathrm{Q}^2 \times M_r N_r \mathrm{Q}^2$ MIMO system [9]. In a sub-connected hybrid AoSA architecture, each SA is driven by a single RF chain, and analog beamforming is configured at the level of AEs in each SA (the SA is effectively the smallest addressable unit for spatial multiplexing). The simplified frequency-domain MIMO system model (at the level of SAs) can thus be expressed as

$$\mathbf{y} = \mathbf{H}\mathbf{x} + \mathbf{w},$$

where $\mathbf{x} \in \mathbb{C}^{M_t N_t \times 1}$ and $\mathbf{y} \in \mathbb{C}^{M_r N_r \times 1}$ are the transmitted and received signals, respectively, $\mathbf{H} \in \mathbb{C}^{M_r N_r \times M_t N_t}$ is the channel matrix (we assume perfect channel state information), and $\mathbf{w} \in \mathbb{C}^{M_r N_r \times 1} \sim \mathcal{CN}(\mathbf{0}_N, \mathbf{\Gamma})$ is the additive white Gaussian noise (AWGN) vector of power σ^2 ($\mathbf{\Gamma} = \sigma^2 \mathbf{I}_{M_r N_r}$). Each element $h_{m_r n_r, m_t n_t}$ of $\mathbf{H}$ defines the channel response between transmitting SA (m_r, n_r) and receiving SA (m_t, n_t) ($m_r \in \{1, \cdots, M_r\}$, $n_r \in \{1, \cdots, N_r\}$, $m_t \in \{1, \cdots, M_t\}$, and $n_t \in \{1, \cdots, N_t\}$), and is expressed as

$$h_{m_r n_r, m_t n_t} = \mathbf{a}_r^{\mathrm{H}}(\phi_r, \theta_r) G_r \alpha_{m_r n_r, m_t n_t} G_t \mathbf{a}_t(\phi_t, \theta_t),$$

where $\mathbf{a}_t$ and $\mathbf{a}_r$ are the transmit and receive SA steering vectors, G_t and G_r are the transmit and receive antenna gains, and ϕ_t,θ_t and ϕ_r,θ_r are the transmit and receive azimuth and elevation angles of departure and arrival, respectively (check [7] for details). The path gain is

$$\alpha_{m_r n_r, m_t n_t} = \frac{c_0}{4\pi f d_{m_r n_r, m_t n_t}} e^{-\frac{k(f)}{2} d_{m_r n_r, m_t n_t}} e^{-j\frac{2\pi}{c_0} f\, d_{m_r n_r, m_t n_t}},$$

where f is the frequency of operation, c_0 is the speed of light in free space, $k(f)$ is the frequency-dependent absorption coefficient, and $d_{m_r n_r, m_t n_t}$ is the distance between the transmitting and receiving SAs.
Denoting by D be the distance between the centers of the transmitting and receiving AoSAs, $d_{m_r n_r, m_t n_t}$ can be expressed as

$$d_{m_r n_r, m_t n_t} = \sqrt{D^2 + \Delta^2((m_r - m_t)^2 + (n_r - n_t)^2)}.$$

For a time-slotted transmission with a time slot T, at each time slot, every AE (or SA) can be turned on or off, switched to a specific frequency, or assigned a specific modulation mode and type. The transmission plan comprises three stages: First, we select the active transmitting SAs. Then, we choose the modulation mode (PBM/CBM) for the active SAs. Finally, we select the corresponding communication frequency and the modulation type (an instance of M-QAM or M-PSK). The Gaussian pulse of PBM is expressed as $p(t) = a e^{-(t-b)^2/(2{T_p}^2)}$, where t denotes time, and a, b, and T_p are the amplitude, center, and spread of the pulse, respectively (pulse duration $T_p < T$). Similarly, the raised cosine pulse of CBM is expressed as $q(t) = \mathrm{sinc}\,(t/T)\,(\cos(\pi\alpha t/T)) \,/\left(1-(2\alpha t/T)^2\right)$, for a roll-off factor ($0 \le \alpha < 1$), where $\mathrm{sinc}(\cdot)$ is the sampling function.

Let $\hat{p}(f)$ be the Fourier transform of $p(t)$, expressed as

$$\hat{p}(f) = a T_p \sqrt{2\pi} e^{-2j\pi b f} e^{-2\pi^2 f^2 {T_p}^2},$$

and let $\mathcal{F} = \{f_1, f_2, \ldots, f_S\}$ be the set of absorption-free carrier frequencies available for transmission ($\forall f \in \mathcal{F}$, $k(f) \approx 0$). Furthermore, let $\mathcal{Q} = \{M_1, M_2, \ldots, M_Q\}$ be the set of Q possible modulation types (M-QAMs and M-PSKs), and denote by C_q ($q \in \{1, \ldots, Q\}$) the set of constellation points in M_q. We define for each transmitting SA $i \in \{1, \ldots, M_t N_t\}$, the signal vector that is transmitted at instant k, $\mathbf{u}_i[k]$, over the frequency components of $\mathcal{F}$. Let $\hat{p}[s] = \hat{p}(f_s)$ ($s \in \{1, \ldots, S\}$), and denote by $a_i[k] \in \{0, 1\}$ and $b_i[k] \in C_q$ the sequences of transmitted symbols in PBM and CBM, respectively, for each component i of the transmitted vector. We denote by I_i the frequency index of the CBM-transmitting SA i (one carrier per SA), and we define the vector $\mathbf{u}_i[k]$ as

$$\mathbf{u}_i[k] = \left[x_{i,1}[k], \ldots, x_{i,S}[k]\right]^{\mathrm{T}} \tag{1}$$

$$x_{i,s}[k] = \begin{cases} 0 & (\text{No signal}/H_0^{(i)}) \\ a_i[k]\hat{p}[s] & (\text{PBM}/H_1^{(i)}) \\ 0 & (\text{CBM}/H_2^{(i)}) \text{ and } s \neq I_i \\ b_i[k] & (\text{CBM}/H_2^{(i)}) \text{ and } s = I_i, \end{cases} \tag{2}$$

with $H_0^{(i)}$, $H_1^{(i)}$, and $H_2^{(i)}$ being the corresponding hypotheses of no signal, PBM signal, and CBM signal, respectively.

Let $\mathbf{x}_s[k] = \left[x_{1,s}[k], x_{2,s}[k], \ldots, x_{M_t N_t, s}[k]\right]^{\mathrm{T}} \in \mathbb{C}^{M_t N_t}$ be the transmitted symbol vector at frequency f_s and instant k. The frequency-domain received signal can be expressed as

$$\mathbf{y}_s[k] = \mathbf{H}_s \mathbf{x}_s[k] + \mathbf{w}_s[k], \tag{3}$$

where $\mathbf{H}_s$ is the channel response at frequency f_s and $\mathbf{w}_s[k] \in \mathbb{C}^{M_r N_r}$ is the complex AWGN. This frequency-domain representation is motivated by three observations:

1) Decoupling MIMO signals via channel inversion is much simpler when the channel responses at specific carrier frequencies are readily available. Alternative time-domain solutions are significantly more complex [1].
2) Wide-bandwidth PBM is subject to a high noise factor at the receiver. Furthermore, an additional absorption-induced noise factor arises in THz PBM [4]. The fact that CBM and PBM signals are subject to different noise powers complicates the analyses, and simply neglecting this difference and assuming equal noise powers, as in [10], is not accurate. In our frequency-domain solution, parameter estimation is conducted by only examining the narrowband signals over the carrier frequencies of interest, which validates the assumption of equal PBM and CBM noise variances.
3) Depending on the choice of carriers $\mathcal{F}$, we differentiate between two scenarios: A scenario in which carriers are chosen randomly, and a scenario in which the selected frequencies guarantee channel near-orthogonality. The latter proposed approach significantly enhances performance and reduces complexity in frequency-domain solutions. The relation between channel orthogonality and the separation between SAs as a function of the communication range D and operating frequency is highlighted in [7]. In particular, the frequencies that ensure orthogonality given a fixed spacing Δ are
$$f = zDc/M\Delta^2, \tag{4}$$
for odd values z, and assuming $M_r = N_r = M_t = N_t = M$.

III. Proposed Antenna Index and Modulation Mode Detection

A. Proposed Solution

To estimate the modulation mode of each symbol, we first decouple the received frequency-domain symbols (3). We propose using either of the two linear channel equalizers, zero forcing (ZF) or minimum mean square error (MMSE) (MMSE outperforms ZF in the case of ill-conditioned channels). In the following, we only consider ZF for simplicity, where we multiply $\mathbf{y}_s$ by the pseudo inverse of the channel matrix $\mathbf{H}_s^+ = \left(\mathbf{H}_s^{\mathrm{H}}\mathbf{H}_s\right)^{-1}\mathbf{H}_s^{\mathrm{H}}$, and compute an estimate of $\mathbf{x}_s$:

$$\tilde{\mathbf{x}}_s[k] = \left(\mathbf{H}_s^+\right)\mathbf{y}_s[k] = \mathbf{x}_s[k] + \left(\mathbf{H}_s^+\right)\mathbf{w}_s[k] = \mathbf{x}_s[k] + \tilde{\mathbf{w}}_s[k],$$

where $\tilde{\mathbf{w}}_s[k] = [\tilde{w}_{1,s}[k], \ldots, \tilde{w}_{M_tN_t,s}[k]]^{\mathrm{T}} = \left(\mathbf{H}_s^+\right)\mathbf{w}_s[k]$ is the modified noise vector.

For every s, $\mathbf{H}_s^+$ is computed once and used in K equalizations. Therefore, for each i, we obtain an estimate of $x_{i,s}[k]$:

$$\tilde{x}_{i,s}[k] = \begin{cases} \tilde{w}_{i,s}[k] & H_0^{(i)} \\ a_i[k]\hat{p}[k] + \tilde{w}_{i,s}[k] & H_1^{(i)} \\ \tilde{w}_{i,s}[k] & H_2^{(i)} \text{ and } s \neq I_i \\ b_i[k] + \tilde{w}_{i,s}[k] & H_2^{(i)} \text{ and } s = I_i. \end{cases}$$

The price to pay in pre-processing is an increase in computational complexity, as each equalization involves matrix multiplication and inversion. Nevertheless, as THz channels are typically flat [4], the equalization matrices can be computed offline and stored in memory. Furthermore, fast channel matrix updates can be applied to account for variations over both time and frequency; limited updates can account for variations in channel components over neighboring frequencies.

After decoupling the received signals, the estimated transmitted symbols of (1) and (2) for each SA are fed as an inputs to an energy-based classifier to decide on the correct hypothesis. We define two thresholds, η_1 and η_2, to detect transmission and to differentiate between PBM and CBM, respectively, for each SA $i \in \{1, \ldots, M_tN_t\}$. Using N received symbols, we compute $\bar{P}_{i,s} = \frac{1}{N}\sum_{n=0}^{N-1}\left|\tilde{x}_{i,s}[n]\right|^2$. Hypothesis testing then follows as

$$\begin{cases} P_i \leq \eta_1 & \Rightarrow H_0^{(i)} \\ \eta_1 < P_i \leq \eta_2 & \Rightarrow H_1^{(i)} \\ P_i > \eta_2 & \Rightarrow H_2^{(i)}, \end{cases}$$

$$P_i = \max_{s\in\{1\ldots S\}} \bar{P}_{i,s},$$

where N, η_1 and η_2 are design parameters that can be optimized (the energy of CBM is typically larger than that of PBM [10]). Note that selecting the maximum power outperforms summing over powers which accumulates noise components. Furthermore, this approach is favored because its computations are identical to those required by the subsequent frequency detection stage, significantly reducing the computations.

B. Performance Analysis

We define the random variables $A_{i,s} = N\bar{P}_{i,s} = \sum_{n=0}^{N-1}\left|\tilde{x}_{i,s}[n]\right|^2$ and $A_i = \max_{s\in\{1\ldots S\}} A_{i,s} = NP_i$. A closed form expressions of the cumulative distribution functions $F_{A_{i,s}}$ and F_{A_i} of $A_{i,s}$ and A_i, respectively, are derived in Appendix A. We next define the three types of error:

- Type-I: the probability of detecting a transmission given that there is no transmission: $P_{\mathrm{err},0}^{(i)}$
- Type-II: the probability of detecting no transmission or CBM given that PBM is transmitted: $P_{\mathrm{err},1}^{(i)}$
- Type-III: the probability of detecting no transmission or PBM given that CBM is transmitted: $P_{\mathrm{err},2}^{(i)}$

Hence, we have

$$P_{\mathrm{err},m_i}^{(i)} = \Pr\left(\bigcup_{v\neq m_i} H_v^{(i)} | H_{m_i}^{(i)}\right),$$

for $m_i, v \in \{0,1,2\}$. We define the set of all possible transmission plan combinations as

$$\mathcal{A} = \left\{ \bigcup_{i=1}^{M_tN_t} H_{m_i}^{(i)}; (m_1, m_2, \ldots, m_{M_tN_t}) \in \{0,1,2\}^{M_tN_t} \right\}.$$

The total error probability for modulation mode detection can then be expressed as

$$P_{\mathrm{err,MD}} = \sum_{\mathcal{A}} \Pr\left(\bigcup_{i=1}^{M_tN_t} H_{m_i}^{(i)}\right)\left(\frac{1}{M_tN_t}\sum_{i=1}^{M_tN_t} P_{\mathrm{err},m_i}^{(i)}\right),$$

where $\Pr\left(\bigcup_{i=1}^{M_tN_t} H_{m_i}^{(i)}\right)$ is the prior probability of having the transmission plan $H_{m_1}^{(1)}, H_{m_2}^{(2)}, \ldots, H_{m_{M_tN_t}}^{(M_tN_t)}$. Assuming uniform priors, the error probabilities are (see Appendix B for proofs):

$$\begin{aligned} P_{\mathrm{err},0}^{(i)} &= 1 - F_{A_i}\left(N\eta_1 | H_0^{(i)}\right) \\ P_{\mathrm{err},1}^{(i)} &= 1 + F_{A_i}\left(N\eta_1 | H_1^{(i)}\right) - F_{A_i}\left(N\eta_2 | H_1^{(i)}\right) \\ P_{\mathrm{err},2}^{(i)} &= F_{A_i}\left(N\eta_2 | H_2^{(i)}\right). \end{aligned}$$

IV. Proposed Frequency Detection

For each CBM symbol, we estimate the corresponding carrier frequency. We denote by $\Omega \subset \{1, \ldots, M_t \times N_t\} \times \{1, \ldots, S\}$ the set of CBM SA indices and their corresponding frequency indices, and by $\tilde{I}_l$ the estimated frequency index for SA l ($(l, I_l) \in \Omega$). Similarly, $\forall s \in \{1, \ldots, S\}$, we have

$$\bar{P}_{l,s} = \begin{cases} \dfrac{1}{N}\displaystyle\sum_{n=0}^{N-1}\left|\tilde{w}_{l,s}[n]\right|^2 & s \neq I_l \\ \dfrac{1}{N}\displaystyle\sum_{n=0}^{N-1}\left|b_l[n] + \tilde{w}_{l,s}[n]\right|^2 & s = I_l. \end{cases}$$

The receiver then estimates the carrier frequency index

$$\tilde{I}_l = \arg\max_{s\in\{1,\ldots,S\}} \{\bar{P}_{l,s}\}.$$

Let $V = m_1, \ldots, m_{M_tN_t} \in \{0,1,2\}^{M_tN_t}$. The corresponding error probability of frequency detection (which can be computed empirically) can be expressed as

$$P_{\mathrm{err,FD}} = \sum_{\mathcal{A}} \Pr\left(\bigcup_{i=1}^{M_tN_t} H_{m_i}^{(i)}\right) g(\Omega(V)) \times \tag{5}$$

$$\sum_{(l,s)\in\Omega(V)} \Pr(f_s) \sum_{q=1}^{Q} \Pr(M_q|f_s)\times$$
$$\sum_{\substack{b[1],\ldots,b[N]\\ \in C_q^N}} \Pr(b[0],\ldots,b[N-1]|f_s,M_q)\Pr(\tilde{I}_l \neq I_l|I_l=s),$$

where $g(\cdot)$ is the probability of selecting an element of Ω:

$$g(\Omega(V)) = \begin{cases} \dfrac{1}{|\Omega(V)|} & \Omega \neq \emptyset \\ 0 & \Omega = \emptyset. \end{cases}$$

V. Proposed Modulation Classification

In the final stage, modulation classification is executed over carrier-based signals, to discriminate between the used M-PSKs and M-QAMs. All constellations are considered to have unit energy ($\forall q \in \{1,\ldots,Q\}, \psi \in C_q, \mathbb{E}\left[\psi\psi^{\mathrm{H}}\right] = 1$). Hence, for each $(l, I_l) \in \Omega$ we have

$$\tilde{\mathbf{u}}_{l,I_l} = [\tilde{x}_{l,I_l}[0],\ldots,\tilde{x}_{l,I_l}[K-1]]^{\mathrm{T}}, \quad (6)$$
$$\tilde{x}_{l,I_l}[k] = b_l[k] + \tilde{w}_{l,I_l}[k]$$

Note that $\tilde{\mathbf{u}}_{l,I_l}$ is composed of symbols from a specific constellation in $\mathcal{Q}$, that are corrupted by a zero-mean noise.

Modulation classifiers are typically likelihood-based and feature-based. While computing optimal likelihood functions is computationally expensive, low-complexity feature-based classifiers [11] exploit the characteristics of the signal, such as its amplitude, moments, and cyclic cumulants to detect the modulation type efficiently. These approaches can be extended to MIMO scenarios [12]. Note that in [10], only for a single-input single-output scenario, THz modulation modes (PBM versus CBM) are detected via feature-based energy detectors, and modulation types (M-QAM and M-PSK) are detected via symmetric Kullback-Leibler divergence, where the received signal is represented in a Gaussian mixture model.

After symbols are decoupled, an arbitrary modulation classifier can be used. In the following, we utilize high-order cumulants, which have been successfully used in low-complexity feature-based classification methods [11]. The reference n^{th}-order cumulant, κ_n, is calculated as an average cumulant of noise-free constellation symbols, assuming equiprobable symbols with unit variance. We use the K random values in $\tilde{\mathbf{u}}_{l,I_l}$ (6) to estimate the fourth-order cumulant, assuming that the first moment is $\tilde{\mu}_1 = 0$ (due to constellation symmetry and zero-mean noise). Hence, we have $\tilde{\kappa}_4 = \tilde{\mu}_4 - 3(\tilde{\mu}_2)^2$, where $\tilde{\mu}_4$ and $\tilde{\mu}_2$ are an estimate of the 4^{th} and 2^{nd} central moments. These moments can simply be computed as $\tilde{\mu}_m = \frac{1}{K}\sum_{k=0}^{K-1}\left(\tilde{x}_{l,I_l}[k]\right)^m$, for $m \in \{2,4\}$. The decision on the modulation mode $\tilde{M}$ can then be made using the minimum Euclidean distance criterion as

$$\tilde{M} = \arg\min_{M_q\in\mathcal{Q}} \left|\kappa_{M_q} - \tilde{\kappa}_4\right|,$$

where κ_{M_q} is the reference fourth-order cumulant of modulation M_q. We denote by $P_{\mathrm{err,MC}}$ the error probability of modulation classification (empirically computed as in (5)).

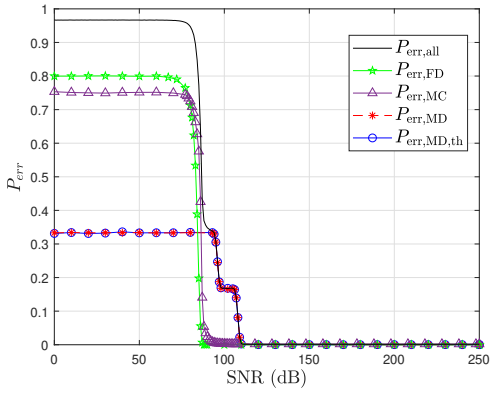

Fig. 1: Error probabilities: Orthogonal scenario.

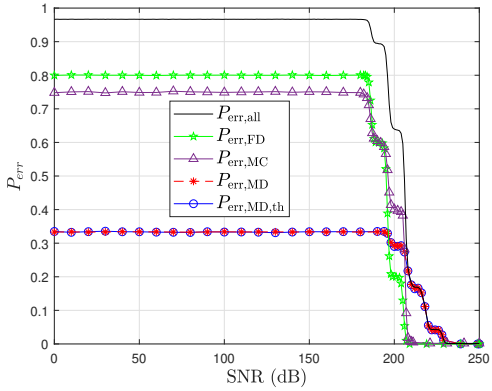

Fig. 2: Error probabilities: Non-orthogonal scenario.

VI. Simulation Results and Discussion

We simulate the proposed solutions following the system model of Sec. II for orthogonal (by design) and non-orthogonal channels. For convenience, we set the distance between the transmitter and the receiver to a virtual $D = 1$ m, assuming that the combination of antenna gains and beamforming (array) gains are capable of compensating the path loss at larger distances. We further set the transmission parameters of the Gaussian pulse to $a = 1$, $b = 0$, and $T_p = 20$ fs, and configure the transceivers to $M_t = N_t = M_r = N_r = M = 8$, with $\Delta = 1$ cm. We use $\mathcal{F}_1$ and $\mathcal{F}_2$ as the sets of orthogonal and non-orthogonal frequencies, respectively. $\mathcal{F}_1$ is defined from (4) for $z \in \{1,3,5,7,9\}$, and $\mathcal{F}_2$ is uniformly distributed over the same range as $\mathcal{F}_2 = \{0.5, 1, \ldots, 2.5\,\mathrm{THz}\}$. We further set the modulation schemes to $\mathcal{Q} = \{\mathrm{BPSK}, \text{4-QAM}, \text{8-PSK}, \text{16-QAM}\}$.

We run an extensive Monte Carlo simulation ($\mathcal{N} = 20000$ trials) in which we randomly vary the transmission plan of each SA. We use the thresholds $\eta_1 = 0.005$ and $\eta_2 = 0.08$, and set $K = 500$ and $N = 20$. Figures 1 and 2 show the overall error probabilities versus signal-to-noise ratio (SNR $= 1/\sigma^2$), alongside the error probabilities of each detection stage. When computing the error probabilities of a particular stage (not the overall probabilities), we assume correct estimation on the previous stages (no propagation of error). We also illustrate the theoretical modulation mode detection performance, which is shown to match the simulations.

We observe that perfect THz parameter estimation is fea-

sible at sufficient SNR values, even when low-complexity feature-based estimation schemes are used in all stages. The high SNR values are caused by the very high losses at THz frequencies, where we assumed unity antenna gains. High antenna and array gains can thus bring these SNR values to normal regions. In fact, it is only through these gains that real THz communications can be realized beyond nano-communications. We notice that the first stage of detection is affected by the threshold values, where at low SNR, the modulation detector always decides on the CBM hypothesis; optimizing the choice of thresholds is part of future work. Forcing channel orthogonality in frequency planning at transmission is shown to achieve a 100 dB gain compared to random frequency allocation. This is a result of reduced inter-stream correlation under near-orthogonality.

VII. Conclusions

In this letter, we investigate a fully-adaptive THz-band system that enables efficient reconfigurable THz communication scenarios. We propose hierarchical low-complexity estimators that recover the modulation modes, modulation types, frequencies of operation, and active antennas' indices. We demonstrate the effectiveness of the proposed solutions via theoretical performance analyses and closely-matching extensive simulation results. As an extension, we plan to explore joint parameter estimation and data detection, as well as machine learning techniques for large-scale joint parameter estimation.

Appendix A
Deriving cumulative distribution functions

For a deterministic THz channel, the covariance matrix of the modified noise vector $\tilde{\mathbf{w}}_s[k]$ is

$$\begin{aligned}\operatorname{cov}(\tilde{\mathbf{w}}_s[k]) &= \left(\mathbf{H}_s^{+}\right)\operatorname{cov}(\mathbf{w}_s[k])\left(\mathbf{H}_s^{+}\right)^{\mathrm{H}}\\ &= \left(\mathbf{H}_s^{\mathrm{H}}\mathbf{H}_s\right)^{-1}\mathbf{H}_s^{\mathrm{H}}\sigma^2\mathbf{I}_{M_r N_r}\mathbf{H}_s\left(\mathbf{H}_s^{\mathrm{H}}\mathbf{H}_s\right)^{-1} = \sigma^2\left(\mathbf{H}_s^{\mathrm{H}}\mathbf{H}_s\right)^{-1}.\end{aligned}$$

Hence, $\tilde{\mathbf{x}}_s[k]|\mathbf{x}_s[k] \sim \mathcal{CN}(\mathbf{x}_s[k], \mathbf{\Gamma}_s)$, where $\mathbf{\Gamma}_s = \sigma^2\left(\mathbf{H}_s^{\mathrm{H}}\mathbf{H}_s\right)^{-1}$. Denote by $\Gamma_{s,i}$ the i^{th} diagonal element of $\mathbf{\Gamma}_s$ ($i \in \{1,\ldots,M_t N_t\}$), i.e., the variance of $\tilde{x}_{i,s}[k]$, we have $\tilde{x}_{i,s}[k]|x_{i,s}[k] \sim \mathcal{CN}(x_{i,s}[k], \Gamma_{s,i})$. Define:

$$\begin{aligned}\mathbf{z}_{i,s} &\in \mathbb{C}^N = \left[\tilde{x}_{i,s}[0]\tilde{x}_{i,s}[1]\ldots\tilde{x}_{i,s}[N-1]\right]^{\mathrm{T}}\\ \boldsymbol{\nu}_{i,s} &\in \mathbb{C}^N = \left[x_{i,s}[0]x_{i,s}[1]\ldots x_{i,s}[N-1]\right]^{\mathrm{T}}\\ \mathbf{R}_{i,s} &\in \mathbb{C}^{N\times N} = \Gamma_{s,i}\mathbf{I}_N.\end{aligned}$$

For each SA and frequency index, the symbols are independently chosen over time; hence, for a deterministic line-of-sight channel, $\tilde{x}_{i,s}[0], \tilde{x}_{i,s}[1]\ldots,\tilde{x}_{i,s}[N-1]$ are also independent. We thus have $\mathbf{z}_{i,s} \sim \mathcal{CN}(\boldsymbol{\nu}_{i,s}, \mathbf{R}_{i,s})$. Therefore, $A_{i,s}$ can be expressed in the quadratic form $A_{i,s} = \mathbf{z}_{i,s}^{\mathrm{H}}\mathbf{Q}\mathbf{z}_{i,s}$, for a Hermitian matrix $\mathbf{Q}=\mathbf{I}_N$. We next seek an explicit expression for the distribution of $A_{i,s}$. Under $H_0^{(i)}$, $\boldsymbol{\nu}_{i,s}=0\ \forall s\in\{1\ldots S\}$. Also, if CBM is used, then $\boldsymbol{\nu}_{i,s}=\mathbf{0}_N\ \forall s\in\{1\ldots S\}\setminus I_i$. In all these cases, the distribution of $A_{i,s}$ is $\chi^2(2N)$ multiplied by $\Gamma_{s,i}/2$. Let $X\sim\chi^2(2N)$ and F_X be its CDF, we have

$$F_{A_{i,s}}(a) = \Pr\left(A_{i,s}\le a\right) = \Pr\left(X \le \frac{2a}{\Gamma_{s,i}}\right) = F_X\left(\frac{2a}{\Gamma_{s,i}}\right).$$

In the other cases where $\boldsymbol{\nu}_{i,s} \neq \mathbf{0}_N$, we define $Y_{i,s}$ as $\chi^2(2N,\lambda_{i,s})$, where $\lambda_{i,s} = \frac{2}{\Gamma_{s,i}}\sum_{n=0}^{N-1}\left|\nu_{i,s}\right|^2$, and we have

$$F_{A_{i,s}}(a) = \Pr\left(A_{i,s}\le a\right) = \Pr\left(Y_{i,s} \le \frac{2a}{\Gamma_{s,i}}\right) = F_{Y_{i,s}}\left(\frac{2a}{\Gamma_{s,i}}\right).$$

The CDF of A_i can then be expressed as

$$F_{A_i}(a) = \Pr(A_{i,1}\le a,\ldots,A_{i,S}\le a) = \prod_{s=1}^{S}\Pr(A_{i,s}\le a) = \prod_{s=1}^{S}F_{A_{i,s}}(a).$$

Appendix B
Deriving error probabilities

$$\begin{aligned}P_{\mathrm{err},0}^{(i)} &= \Pr\left(H_1^{(i)}\bigcup H_2^{(i)}|H_0^{(i)}\right) = \Pr\left(H_1^{(i)}|H_0^{(i)}\right) + \Pr\left(H_2^{(i)}|H_0^{(i)}\right)\\ &= \Pr(\eta_1 < P_i \le \eta_2|H_0^{(i)}) + \Pr(P_i > \eta_2|H_0^{(i)})\\ &= \Pr(P_i > \eta_1|H_0^{(i)}) = \Pr\left(\frac{A_i}{N} > \eta_1|H_0^{(i)}\right)\\ &= \Pr\left(A_i > N\eta_1|H_0^{(i)}\right) = 1 - \Pr\left(A_i < N\eta_1|H_0^{(i)}\right)\\ &= 1 - F_{A_i}\left(N\eta_1|H_0^{(i)}\right).\end{aligned}$$

$P_{\mathrm{err},1}^{(i)}$ and $P_{\mathrm{err},2}^{(i)}$ are similarly derived.

References

[1] M. H. Loukil, H. Sarieddeen, M.-S. Alouini, and T. Y. Al-Naffouri, "Terahertz-band MIMO systems: Adaptive transmission and blind parameter estimation." [Online]. Available: http://hdl.handle.net/10754/656859

[2] N. Rajatheva *et al.*, "Scoring the terabit/s goal: Broadband connectivity in 6G," *arXiv preprint arXiv:2008.07220*, 2020.

[3] H. Sarieddeen, N. Saeed, T. Y. Al-Naffouri, and M.-S. Alouini, "Next generation terahertz communications: A rendezvous of sensing, imaging, and localization," *IEEE Commun. Mag.*, May 2020.

[4] H. Sarieddeen, M.-S. Alouini, and T. Y. Al-Naffouri, "An overview of signal processing techniques for terahertz communications," *arXiv preprint arXiv:2005.13176*, 2020.

[5] K. Sengupta, T. Nagatsuma, and D. M. Mittleman, "Terahertz integrated electronic and hybrid electronic-photonic systems," *Nature Electronics*, vol. 1, no. 12, p. 622, 2018.

[6] L. Ju, B. Geng, J. Horng, C. Girit, M. Martin, Z. Hao, H. A. Bechtel, X. Liang, A. Zettl, Y. R. Shen *et al.*, "Graphene plasmonics for tunable terahertz metamaterials," *Nature nanotechnology*, vol. 6, no. 10, p. 630, 2011.

[7] H. Sarieddeen, M. Alouini, and T. Y. Al-Naffouri, "Terahertz-band ultra-massive spatial modulation MIMO," *IEEE J. Sel. Areas Commun.*, vol. 37, no. 9, pp. 2040–2052, Sep. 2019.

[8] J. M. Jornet and I. F. Akyildiz, "Femtosecond-long pulse-based modulation for terahertz band communication in nanonetworks," *IEEE Trans. Commun.*, vol. 62, no. 5, pp. 1742–1754, May 2014.

[9] H. Sarieddeen, M. M. Mansour, and A. Chehab, "Large MIMO detection schemes based on channel puncturing: Performance and complexity analysis," *IEEE Trans. Commun.*, vol. 66, no. 6, pp. 2421–2436, Jun. 2018.

[10] M. O. Iqbal, M. M. Ur Rahman, M. A. Imran, A. Alomainy, and Q. H. Abbasi, "Modulation mode detection and classification for in vivo nano-scale communication systems operating in terahertz band," *IEEE Trans. Nanobiosci.*, vol. 18, no. 1, pp. 10–17, Jan. 2019.

[11] M. S. Mühlhaus, M. Öner, O. A. Dobre, H. Jaekel, and F. Jondral, "Automatic modulation classification for MIMO systems using fourth-order cumulants," *Proc. IEEE Vehic. Technol. Conf. (VTC)*, pp. 1–5, Sep. 2012.

[12] H. Sarieddeen, M. M. Mansour, L. M. A. Jalloul, and A. Chehab, "Likelihood-based modulation classification for MU-MIMO systems," in *Proc. IEEE Global Conf. on Signal and Inform. Process. (GlobalSIP)*, Dec. 2015, pp. 873–877.